Biomaterials 32 (2011) 5837–5846

Contents lists available at ScienceDirect

Biomaterials

journal homepage: www.elsevier.com/locate/biomaterials

The structural and biological properties of hydroxyapatite-modified titanate nanowire scaffolds

Haixin Zhao [a], Wenjun Dong [a,b,*], Yingying Zheng [a], Aiping Liu [a], Juming Yao [a,**], Chaorong Li [a], Weihua Tang [a], Benyong Chen [a], Ge Wang [b], Zhan Shi [c]

[a] Center for Optoelectronics Materials and Devices, Center for Nanoscience and Noanotechnology, Key Laboratory of Advanced Textile Materials and Manufacturing Technology, Ministry of Education, Engineering Research Center for Eco-Dying & Finishing of Textiles, Zhejiang Sci-Tech University, Hangzhou 310018, PR China
[b] School of Materials Science and Engineering, University of Science and Technology Beijing, Beijing 100083, PR China
[c] State Key Laboratory of Inorganic Synthesis and Preparative Chemistry, College of Chemistry, Jilin University, Changchun 130012, PR China

ARTICLE INFO

Article history:
Received 15 March 2011
Accepted 27 April 2011
Available online 24 May 2011

Keywords:
Scaffold
Hydroxyapatite
Titanate nanowire
Biomaterial

ABSTRACT

Hydroxyapatite-modified titanate nanowire scaffolds as alternative materials for tissue engineering have been developed via a titanate nanowire matrix assisted electrochemical deposition method. The macroporous titanate nanowire matrix on Ti metal was fabricated by a hydrothermal method, and then followed by an electrochemical synthesis of hydroxyapatite nanoparticles on titanate nanowire. The incorporation of titanate nanowire matrix with high oriented hydroxyapatite nanoparticles generates hierarchical scaffolds with highly osteogenic, structural integrity and excellent mechanical performance. As-prepared porous three dimensional interconnected hydroxyapatite-modified titanate nanowire scaffolds, mimicking the nature's extracellular matrix, could provide a suitable microenvironment for tissue cell ingrowth and differentiation. The ceramic titanate nanowire core with HA nanoparticle sheath structure displays superhydrophilicity, which facilitates the cell attachment and proliferation, and induces the *in vitro* tissue-engineered bone. Human osteoblast-like MG63 cells were cultured on the hydroxyapatite-modified titanate nanowire scaffolds, and the results showed that the scaffolds highly promote the bioactivity, osteoconductivity and osteoblast differentiation.

1. Introduction

Due to the donor shortage for autografts, potential risk of disease transmission in allografts and immunological responses, researchers have turned to the artificial bone scaffolds for implantation as bone graft materials [1,2]. Artificial scaffolds can not only serve as a mechanical substrate, but also release structural signals perceived as biologically relevant by both stem and differentiated cells, thus mimicking the *in vivo* microenvironment [3,4]. Specifically, hydroxyapatite ($Ca_{10}(PO_4)_6(OH)_2$, HA) has a composition close to natural bone mineral or hard tissue which is capable of supporting bone growth and osteointegration for bone tissue regeneration [5,6]. Recently, attempts have been made to coat HA nanoparticles on a hard metal substrate via different techniques (e.g., sol–gel process, electrophoretic deposition, and plasma-sprayed) for medical applications [7–9]. Usually, the coating process requires high temperature over 1000 °C to improve the osteoconductive property and reduce the corrosive-wear resistance [10]. However, this heat treatment makes the coating suffer from cracking, loss of adhesion and mechanical stability, which is out of the requirements of clinical use in load-bearing applications like artificial bones or teeth [11,12]. A robust and porous nanowire membrane similar to bone nanostructure scaffold has also been developed directly on metal substrate, which possesses interconnected macropores, ample void space inside and sufficient mechanical strength. The porous nature allows blood vessel transportation and promote cell adherence when the scaffold is introduced into body [13–15]. However, the bioactivity, biocompatibility and toughness of the nanowire scaffolds still need to be improved.

It is well known that the HA nanocrystals are deposited in an orderly manner on the collagen matrix in natural bone [16], in which the highly ordered manner of intrafibrillar mineralization at the nanoscale is responsible for the biomechanical properties of

* Corresponding author. Center for Optoelectronics Materials and Devices, Center for Nanoscience and Noanotechnology, Key Laboratory of Advanced Textile Materials and Manufacturing Technology, Ministry of Education, Engineering Research Center for Eco-Dying & Finishing of Textiles, Zhejiang Sci-Tech University, Hangzhou 310018, PR China. Tel.: +86 571 86843587.
** Corresponding author.
E-mail addresses: wenjundong@zstu.edu.cn (W. Dong), yaoj@zstu.edu.cn (J. Yao).

0142-9612/$ – see front matter © 2011 Elsevier Ltd. All rights reserved.
doi:10.1016/j.biomaterials.2011.04.083

mineralized collagen scaffolds [17]. Bone-like tissue-engineered material, such as silk-based scaffold [18], decellularized osteoblast matrices [19], and polymer-HA composites [20] have been created to mimic certain features of bone. Usually, the porous bioscaffolds, capable of controlling the surface chemistry, could provide a suitable microenvironment for cell differentiation and tissue ingrowth [21–24]. The integration of nanowires with HA nanoparticles, mimiking the natural extracellular matrix for improving the cellular compatibility and mechanical performance, can enhance the bioactivity for cell/tissue attachment, reinforce its osteoconductive property and guide tissue growth, as well as promote bone ingrowth and osteointegration [25,26].

In this paper, a facile method has been developed to fabricate a special hierarchical nano-micro structure scaffold on Ti metal substrate. The macroporous titanate nanowire matrix on Ti metal was fabricated by a hydrothermal method, and then followed by an electrochemical method to deposit hydroxyapatite nanoparticles on titanate nanowires. Proliferation and differentiation of MG63 osteoblast cells on hydroxyapatite-modified titanate nanowire scaffolds were systematically investigated to evaluate the effects of ordered cellular microenvironment for cell growth, the bioactivity of the oriented HA nanocrystals for cell/tissue attachment, and the promotion of osteointegration between the bone and scaffolds.

2. Materials and methods

2.1. Preparation of self-assembled titanate nanowire matrix

The titanate nanowire matrix was prepared based on previously described method [13]. Before the synthesis, titanium plates 20 mm × 10 mm were inserted in 10 mL of acetone at room temperature, ultrasonicated for 15 min, then ultrasonicated for 10 min in 10 mL of absolute ethylalcohol, and rinsed with deionized water thereafter. The Ti substrate was then placed in a Teflon-lined vessel containing 10 mL of 1.0 mol/L NaOH solution. Afterward, the vessel was sealed and then hydrothermally heated at 240 °C for 8 h. Thus-treated Ti substrates, covered by the titanate nanowire matrix, were finally collected, rinsed with deionized water, and dried in air.

2.2. Preparation of hydroxyapatite-modified titanate nanowire scaffolds

The deposition of HA nanostructures on titanate nanowire matrix were carried out on *Zahner elektrik IM6 PVI* model potentiostat/galvanostat in a three-electrode cell with titanate nanowire martix on Ti plate as the working electrode (WE), a platinum plate as the counter electrode (CE), and commercial saturated calomel electrode (SCE) as reference electrode (Supplementary Material Scheme 1) [27,28]. The deposition process was monitored using a SCE with a potential range from 1.0 to 1.3 V, and the current (voltage) was in the range of −5 – −20 mA (−1.0 – −2.0 V) between 25 and 65 °C for 0.5–3 h. The electrolyte solution was composed of modified simulated body fluid (SBF), NaCl: 8.0, $CaCl_2$: 0.14, KCl: 0.40, $NaHCO_3$: 0.35, Glucose: 1.00, KH_2PO_4: 0.10, $MgCl_2 \cdot 6H_2O$: 0.10, $Na_2HPO_4 \cdot 2H_2O$: 0.06, $MgSO_4 \cdot 7H_2O$: 0.06g, respectively [29]. All solutes were dissolved in distilled water (1000 mL) and the pH was adjusted to 7.40–9.30 with $NaHCO_3$ solution.

2.3. Microstructural characterization of hydroxyapatite-modified titanate nanowire scaffolds

Surface topography of the hydroxyapatite-modified titanate nanowire scaffolds was detected on a field emission scanning electron microscope (FESEM; HITACHI S-4800, Japan), and energy dispersive X-ray spectroscopy (EDX) microanalysis probe (LINK) was used for the elemental composition of samples.

Structure and phase composition of the hydroxyapatite-modified titanate nanowire scaffolds was identified by XRD on a D8 Discover X-ray diffractometer (Bruker, AXS, German) at a scanning speed of 0.02°/s with Cu Kα radiation ($\lambda = 0.15405$ nm, 40 mA, 40 kV) at a 2θ range of 20–70°.

The hydroxyapatite-modified titanate nanowire scaffold structure was analyzed on a JEOL-2010 transmission electron microscopy (TEM; Japan) operating at 200 kV. For the preparation of TEM samples, hydroxyapatite nanoparticle modified titanate nanowires were flaked from specimens and ultrasonicated in the absolute ethylalcohol.

Structural and molecular composition of the hydroxyapatite nanoparticle modified titanate nanowire scaffolds was evaluated on a Nicolet 5700 Fourier transform infrared spectroscopy-attenuated total reflection spectrometer (FTIR-ATR; USA) with a resolution of 4 cm^{-1} and a scan number of 32, and the samples were analyzed from 400 to 4000 cm^{-1}.

2.4. pH measurement during the reaction

The pH of the electrolyte solution was measured on a PHSJ-3F laboratory pH-meter (Precision & Scientific Instrument CO., LTD, Shanghai, China). The pH changes during the reaction were investigated for 3 h, and each value was an average of 6 measurements in the same batch.

2.5. In vitro cell culture tests

The human MG63 cells, an osteosarcoma cell line (Shanghai Institute of Biochemistry and Cell Biology, Shanghai, China), were cultured in Dulbecco's Modified Eagles Medium (DMEM) supplemented with 10% fetal bovine serum (FBS) and antibiotics (100 U/ml penicillin, 100 mg/ml streptomycin). MG63 cells were digested using 0.25% trypsin for 3–5 min, centrifuged at 800g for 5 min and resuspended in the medium. Cell numbers were determined by counting via a haemacytometer, and then diluted to the concentration of 1×10^5 cells mL^{-1}. The hydroxyapatite nanoparticle modified titanate nanowire scaffolds and titanate nanowire matrix were immerged in 75% alcohol sterilized under UV irradiation for 1 h in a 24-well culture plates. Subsequently, each sample was washed with phosphate buffered saline (PBS) for 6 times, and dried at room temperature. The culture medium containing MG63 cells of 500 μl was dipped on each culture well, and then cultured in the humidified incubator with 5% CO_2 at 37 °C, and the culture medium was replaced every other day.

2.5.1. Fluorescence microscope of cell morphology

When MG63 cells were cultured for 1d, 3d, 5d and 7d, the culture medium with unattached cells was carefully removed from the culture wells by a pipette, and then the samples were rinsed twice with PBS buffer. The cells on the samples were fixed with 2.5% glutaraldehyde in 0.1 M PBS buffer (pH = 7.4) for 20 min, and permeabilized 3 times with 0.1% Triton X-100 (Beyotime Institute of Biotechnology, China) diluted in PBS for 5 min at room temperature, respectively. For fluorescence imaging, the cytoskeleton of osteoblasts was stained with 500 μl Actin-Tracker Green (phalloidin-FITC, Beyotime Institute of Biotechnology, China; 30 μl phalloidin-FITC in 3 ml 0.1% Triton X-100 PBS) for 60 min at 37 °C. After that, the samples were washed 3 times with 0.1% Triton X-100 diluted in PBS for 5 min at room temperature. Subsequently, the nucleus was counterstained with 4′-6-Diamidino-2-phenylindole DAPI (Beyotime Institute of Biotechnology, China; 5 μg/mL DAPI in MilliQ-water) for 15 min at 37 °C, and rinsed 2 times with 0.1% Triton X-100 PBS. The samples were photographed by a fluorescence microscope (BX51; OLYMPUS, Japan) with B- and G-light excited at 420–485 nm and 460–550 nm, respectively.

2.5.2. Field emission scanning electron microscope of cell morphology

When MG63 cells were cultured for 1, 3, 5 and 7 days, the culture medium with unattached cells was carefully removed from the wells by a pipette, and then rinsed 2 times with PBS buffer. The cells on the samples were fixed with 2.5% glutaraldehyde in 0.1 M PBS buffer (pH = 7.4) for 20 min, and washed 3 times with PBS for 5 min at room temperature. Afterward, each sample was graded dehydration with 10%, 20%, 30%, 50%, 60%, 70%, 80%, 90% and absolutely pure ethylalcohol for 10 min at room temperature, respectively, and then the samples were dried for SEM analysis.

2.5.3. MTT and ALP assay

After 1, 3, 5 and 7 days of co-incubation, the culture medium was removed from each culture well, and the specimens were transferred to new 24-cell culture plates. Subsequently, 100 μl of fresh culture medium and 20 μl of methyl thiazolyl and tetrazolium (MTT) solution (5 mg mL^{-1}) were added to each culture well for a further 4 h, and then the MTT solution was removed. Next, 200 μl of DMSO was added and the determinate was taken at 570 nm in a spectrophotometric microplate reader (Bio-RAD Model 680, USA). The data reported were the mean value of 3 examinations.

The retention of the osteoblastic phenotype at days 1, 3, 5 and 7 was evaluated by measuring the alkaline phosphatase (ALP) activity. After co-incubation, the samples were moved to new 24-well culture plates and washed 2 times with PBS (2%), and digestive juice was added with 5–10 min. Subsequently, the digestive juice was discarded, and the samples were rinsed 2 times with PBS and 500 μl of 0.2% Triton X-100 PBS was added, then a freezing and thawing process was repeated 3 times to extract the intracellular phosphatase. The measurement of the ALP activity in the cell lysates was based on the conversion of colorless *p*-nitrophenyl phosphate into colored *p*-nitrophenol (JianCheng Biotech.). The colour intensity was measured at 520 nm using the UV–*vis* spectrophotometer (DU530, BeckmanCoulter, Inc., Fullerton,. CA). The amount of ALP was quantified by the comparison with a standard sample. The data reported were the mean value of 3 examinations.

2.6. Statistical analysis

All data presented were expressed as mean values ± standard deviations (SD) at a significance level of $p < 0.05$ for each group of samples. After the assessment of significant differences by one-way variance analysis (ANOVA), the differences among the groups were established with *t*-test analysis by a two-population comparison.

3. Results and discussion

3.1. Morphology of hydroxyapatite-modified titanate nanowire scaffolds

The effects of reaction time, electrolyte temperature, pH value and current conditions on the morphology of hydroxyapatite-modified titanate nanowire scaffolds were systematically studied. Fig. 1 shows the FESEM images of HA nanostructure modified titanate nanowire scaffolds with different deposition time. Initial titanate nanowire matrix was composed of interconnected macropores of 2–10 μm in diameter (Supplementary Material Fig. S1). When the electrochemical deposition was carried out for 1 h, laminar HA nanostructure coated titanate nanowires with a relatively poor distribution were obtained (Fig. 1A and A*). When the reaction time was increased to 2 h, most HA laminar structures were developed into nano-corn structures with 50–200 nm in length and 20–50 nm in width around the titanate nanowires (Fig. 1B and B*). When the reaction time was extended to 3 h, dense HA nano-grain structures with a mean length of 150 nm and width of 30 nm covered the titanate nanowires completely to form the ceramic titanate nanowire core with HA nanoparticle sheath structures, which can be described as the "necklace bead model" scaffolds (Fig. 1C and C*). Interestingly, the HA nanoparticles were similar to the mineral phase of bone constituted of HA crystals with a length of about 100 nm, width of 20–30 nm, and thickness of 3–6 nm [30].

The influence of electrolyte temperature on the morphology of the hydroxyapatite nanostructure modified titanate nanowires (pH = 8.60, $I_{appl} = -15$ mA and $t = 3$ h) is shown in Fig. 2. When the electrolyte temperature was 25 °C, laminar HA structures with low population density were deposited on the titanate nanowires (Fig. 2A and A*). When the electrolyte temperature was increased to 37 °C, laminar HA nanostructures were deposited on most titanate nanowires (Fig. 2B and B*). When the temperature was further increased to 65 °C, "necklace bead mode" scaffolds were obtained (Fig. 1C and C*). In addition, the influence of the pH and current were also investigated on the morphology of the HA nanostructures deposited on the titanate nanowire matrix (as shown in Supplementary Material Figs. S2 and S3). Overall, the optimized condition to obtain "necklace bead mode" scaffolds was current of −15 mA, pH of 8.60 and the electrolyte temperature of 65 °C for 3 h. In light of these results, the biocompatible HA nanoparticle modified titanate nanowire scaffolds with macroporous and interconnected structure were fabricated successfully (Fig. 1C and C*), in which the prepared HA nanostructures deposited on titanate nanowire matrix exhibite the structure integrity and cellular compatibility. The incorporation of HA altered scaffold

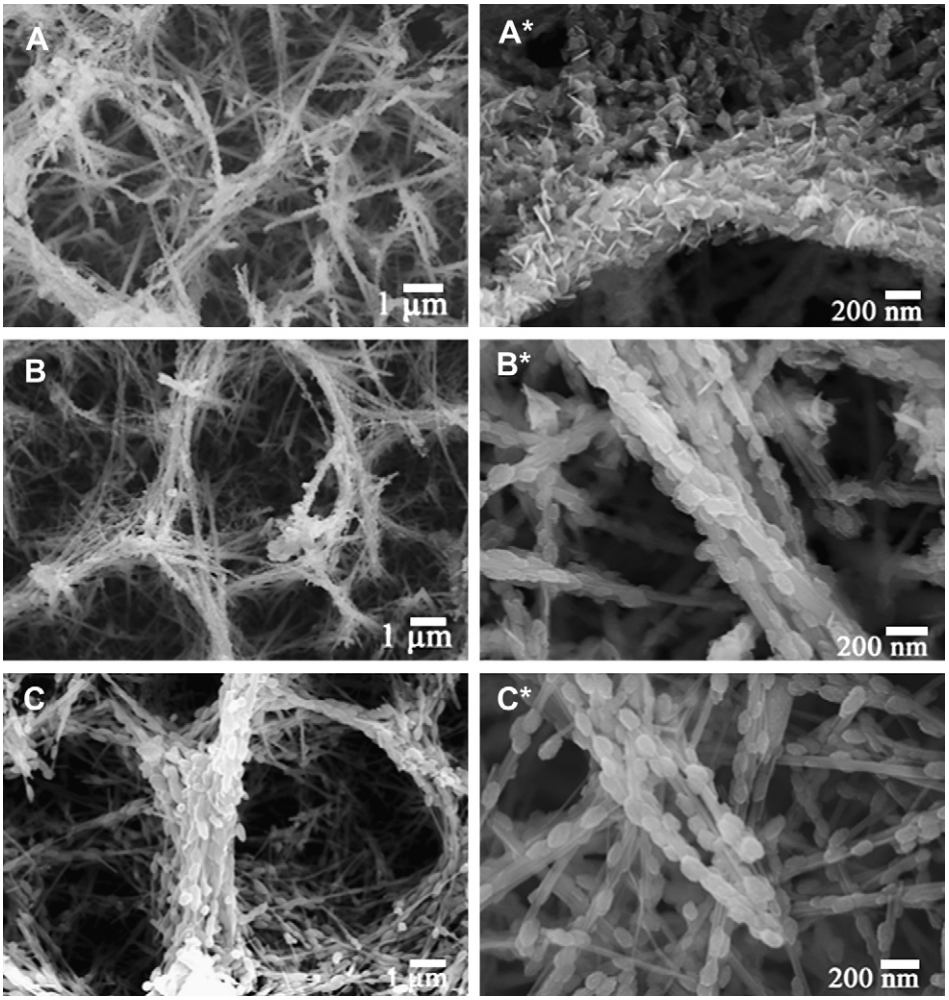

Fig. 1. FESEM images of as-prepared hydroxyapatite-modified titanate nanowire scaffolds with different deposition time: A) 1 h, B) 2 h, C) 3 h. A*–C*) High-magnification FESEM images of A–C, respectively (electrochemical deposition condition: pH = 8.60, $T = 65$ °C and $I_{appl} = -15$ mA).

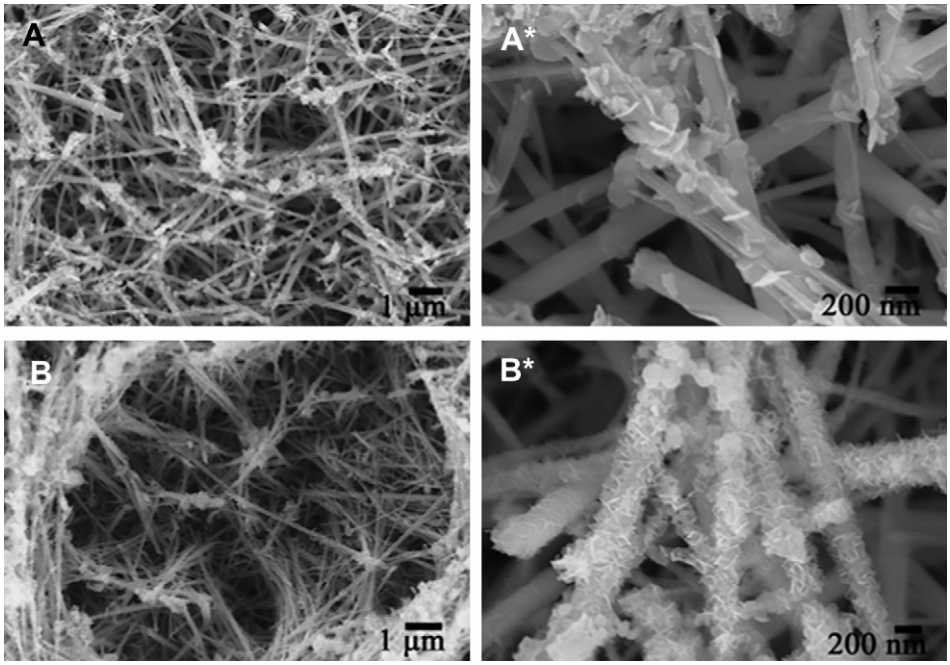

Fig. 2. The influence of electrolyte temperature on hydroxyapatite-modified titanate nanowire scaffolds: A–B) FESEM images of deposition temperature 27 °C and 37 °C. A*–B*) High-magnification images of A–B, respectively (electrochemical deposition condition: pH = 8.60, $I_{appl} = -15$ mA and $t = 3$ h).

surface chemistry, increased surface roughness and stiffness of the titanate nanowire matrix (Supplementary Material Fig. S1), and was very similar to the osteoblast adhesion on the surface characteristics of materials (e.g., topography, chemistry or surface energy).

3.2. Elemental composition and structure of hydroxyapatite-modified titanate nanowire scaffolds

As we know, Mg^{2+} and HCO_3^- are essential for HA nanostructures coated on the scaffolds, which can reduce the size of HA crystals and keep the HA crystals more stabilized on the substrate [31]. So the SBF and pH have been tuned to control the Mg^{2+} and carbonate in the artificial hydroxyapatite nanostructure modified titanate nanowire scaffolds. Interestingly, the HA nanostructures prepared by electrochemical method can simulate the biological apatites, in that, cations such as Mg^{2+}, Na^+ and K^+, and anions such as Cl^- and F^- can be introduced into HA lattice by substitution of Ca^{2+} and OH^- [32]. EDX spectrum of the "necklace bead model" scaffolds is depicted in Fig. 4A, in which sodium (Na), calcium (Ca), phosphorous (P), titanium (Ti), magnesium (Mg), and oxygen (O) elements are present. The elemental analysis result is shown in Table 1, and the Ca/P ratio of 1.62 of the composite scaffolds is similar to the calculated ratio of 1.67 in the HA of natural bone. It also confirms the successful formation of the HA component in the scaffold.

It is worth mentioning that one of the mineral components inside the bones and teeth of the human body is the hexagonal hydroxyapatite (molecular formula: $Ca(2)_6Ca(1)_4(PO_4)_6(OH)_2$, $P6_3/m$) with good biocompatibility property [33]. The XRD pattern of the "necklace bead model" scaffolds reveals that the crystal phase of the HA can be indexed as hexagonal hydroxyapatite (JCPDS 72-1243), with $P6_3/m$ space group symmetry, and the lattice parameters of $a = b = 9.432$ Å, $c = 6.881$ Å, and $\gamma = 120°$ (as shown in Fig. 4B) [34]. The diffraction characteristic peaks at 21.75°, 25.85° and 31.76° are assigned to the (200), (002) and (112) planes of HA crystal. The broadening and overlap of peaks confirm that the obtained HA nanoparticle is similar to natural bone mineral in terms of the poor crystallinity. The HA crystal displays anisotropic growth along the *c*-axis through XRD pattern, since the intensity increase of (002) peak is obviously faster than that of (300) peak. The TEM images of the uniform HA nanostructure coated on the titanate nanowires show that the square-shaped HA crystallite particles with 2 nm in width are oriented deposited on the titanate nanowires (Fig. 4C). TEM images of the "necklace bead model" scaffolds exhibit a clear phase interface between HA nanoparticle and titanate nanowire matrix (Fig. 4D insert), and the ordered HA nanocrystal was bounded by a sheath of crystallites which have likewise parallel orientation structure of natural bone. The HRTEM image of HA nanoparticles on the "necklace bead model" scaffolds shows that the spacing of crystal lattice planes of 0.409 and 0.345 nm matches the (200) and (002) planes of the hexagonal HA, respectively (Fig. 4D). The amorphous crystals and lattice defects on the sheath of HA may be induced by the surface charge property of the titanate nanowires and current interaction in the process of electrochemical reaction. More importantly, the hexagonal hydroxyapatite is thermodynamically relatively stable, which can be deposited on the titanate nanowires directly without further sinter process. The FESEM image and XRD pattern of the sample calcined at 450 °C and 550 °C for 3 h

Table 1
Elemental analysis of the "necklace bead model" composite scaffolds and the hydroxyapatite.

Element and ratio	Experimental	Theroretical[a]
C	1.23	/
O	39.20	59.09
H	N/A	4.54
P	6.35	13.64
Ti	37.13	/
Na	3.05	/
Ca	10.29	22.73
Mg	2.75	/
Ca/P	1.62	1.67

[a] Calculated atomic fractions and Ca/P ratio in the HA ($Ca_{10}(PO_4)_6(OH)_2$).

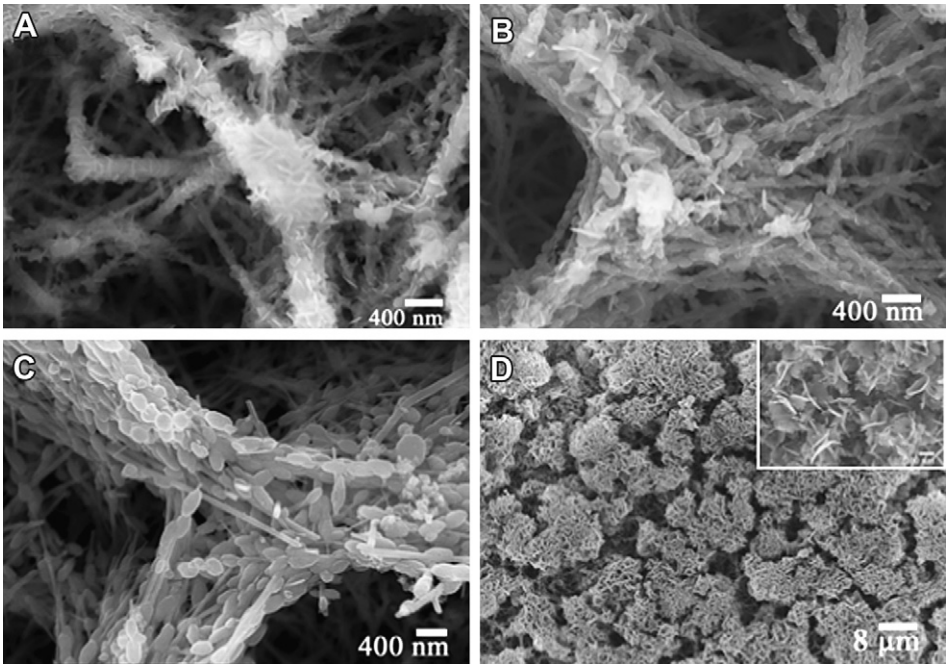

Fig. 3. FESEM images of hydroxyapatite-modified titanate nanowire scaffolds with constant current electrochemical deposition: A–C) the development of the HA on titanate nanowire from laminar to nano-grain structure. D) FESEM images of hydroxyapatite-modified titanate nanowire scaffolds with constant potential electrochemical deposition (pH = 8.60, $T = 65$ °C, $U_{appl} = -2.0$ V and $t = 20$ min).

are similar to the as-prepared of the "necklace bead model" scaffolds (Supplementary Material Figs. S4 and S5).

3.3. FTIR-ATR analysis of hydroxyapatite-modified titanate nanowire scaffolds

FTIR-ATR spectra were collected to confirm the successful synthesis of the hexagonal hydroxyapatite on the titanate nanowire matrix (Fig. 4E). The intense P–O stretching bands ca. 1041 cm^{-1} represent the ν_3 mode of PO_4^{3-} ions in HA, and the adsorption band at 3698 cm^{-1} is due to the presence of OH^- groups [35]. Band located at 872 cm^{-1} corresponds to the ν_2 peak of CO_3^{2-} out-of-plane stretching. Actually, the ν_3 peak of CO_3^{2-} is composed of two bands, 1453 cm^{-1} (type A CO_3^{2-}) and 1417 cm^{-1} (type B CO_3^{2-}), which can be attributed to the CO_3^{2-} substitute for OH^- or PO_4^{3-} ions in the HA crystal [36], and the B-type substitution has been considered as the most close resembling of biological apatites. Further, the lack of a band at 1540 cm^{-1} also confirms the substitution of carbonate for the phosphate group [37]. The presence of carbonate located in type B site contributes to the formation of a poorly crystallized carbonated apatite that has similar features as bone mineral phase [38]. The FTIR-ATR spectra of the "necklace bead model" scaffolds calcined at 450 °C and 550 °C for 3 h show results similar to the as-prepared specimen (Supplementary Material Fig. S6), confirming the successful formation of the hexagonal HA nanoparticles by electrochemical deposition.

3.4. The changes of pH value during the reaction

Usually, hydroxyapatite can be prepared directly with sufficient alkalization in the bath [39], and the concentration of OH^- near the cathode exerts great effects on the formation of HA structure [40,41]. The pH value near the working electrode (titanate nanowire matrix) surface was monitored during the electrochemical deposition process under galvanostatic control (shown in Fig. 4F). When constant current was applied in the HA deposition process, hydroxide ions absorbed on titanate nanowires were derived to form laminar HA nanostructure (Fig. 3A) and the pH value was dropped to 7.85 in 55 min. Subsequently, with the laminar HA nanostructure developing into nanoparticle on the titanate nanowires (Fig. 3B and C), the pH value was increased gradually from 7.85 at 55 min to 8.2 at 140 min. The changes of pH value were attributed to the reduced deposition reaction speed and the OH^- produced by the electrochemical reaction excess than the OH^- consumption of HA formation. In addition, the constant potential electrochemical deposition method would yield HA film to cover the titanate nanowire matrix (Fig. 3D), which destroys the structural integrity of interconnected macropores.

Based on the above results, the electrochemical deposition of HA nanostructures on titanate nanowires can be divided into two steps. First, the hydroxide and phosphate ions were generated around the cathode (titanate nanowire matrix) in the solution (eqs. 1–4) [42]. The surface of titanate nanowires absorbed water to form titanium hydroxide groups, and then calcium cations were attracted to the surface of titanate nanowires. Second, when excess hydroxide ions were present in the solution, the hydroxide and phosphate ions combined Ca^{2+} to produce HA nanocrystals on the surface of titanate nanowires (eq. 5) [43]. In general, the cathodic deposition in the electrolytic solution follows the formulae below:

$$2H_2O + 2e^- \rightarrow H_2 + 2OH^- \quad (1)$$

$$2H_2PO_4^- + 2e^- \rightarrow 2HPO_4^{2-} + H_2 \quad (2)$$

$$2HPO_4^{2-} + 2e^- \rightarrow 2PO_4^{3-} + H_2 \quad (3)$$

$$HPO_4^{2-} + OH^- \rightarrow PO_4^{3-} + H_2 \quad (4)$$

$$10Ca^{2+} + 6PO_4^{3-} + 2OH^- \rightarrow Ca_{10}(PO_4)_6(OH)_2 \quad (5)$$

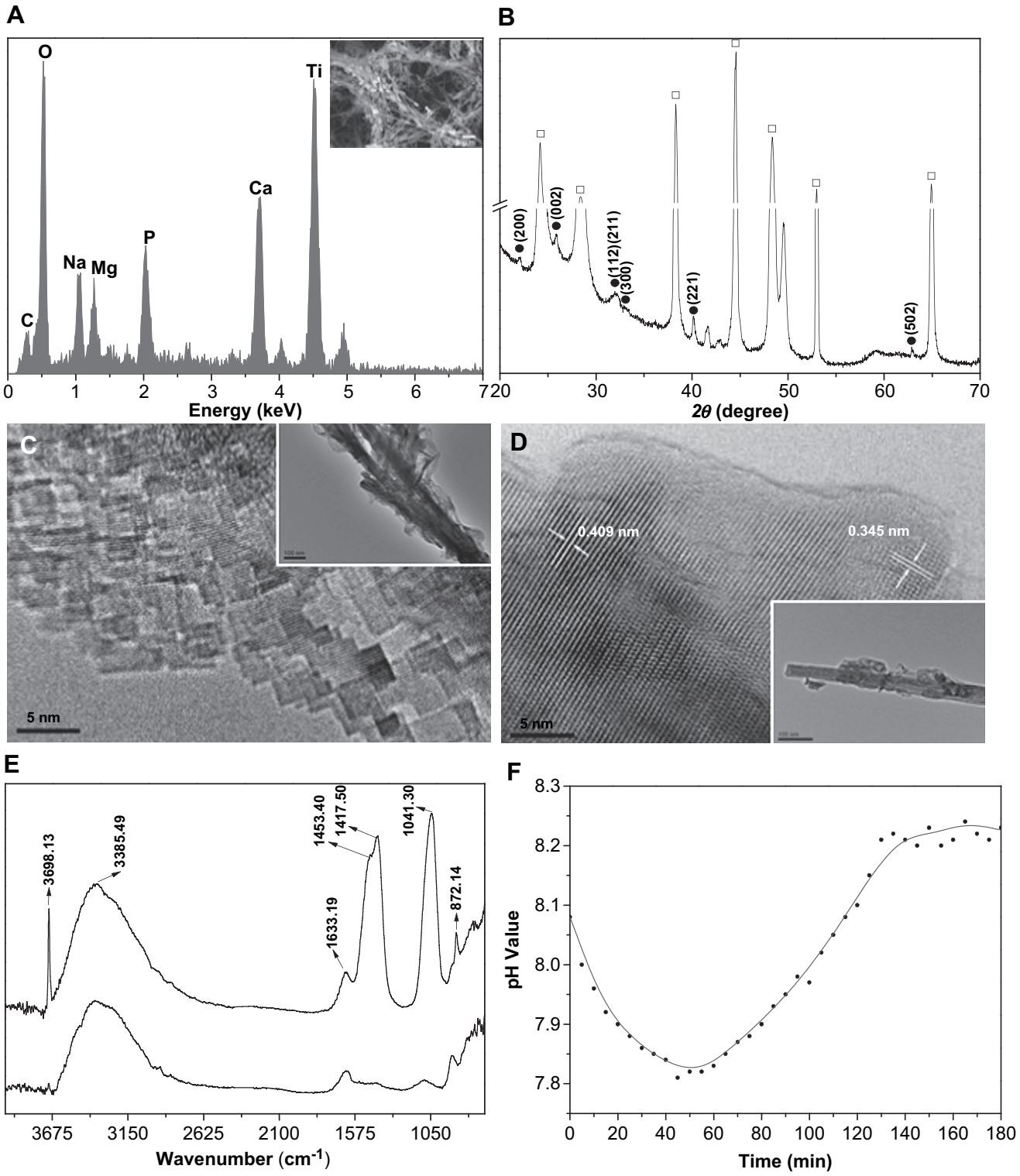

Fig. 4. Evaluation of the EDX, crystalline structure, TEM and FTIR-ATR analysis of the hydroxrapatite-midified titanate nanowire scaffolds: A) EDX analysis of the selected area "necklace bead model" scaffolds. B) XRD pattern of the "necklace bead model" scaffolds. The characteristic peaks for titanate and HA are marked as squares and circles, respectively. C) HRTEM of laminar HA nuclei. The inset shows TEM micrograph of hydroxyapatite nanostructure midified titanate nanowire. D) High-resolution micrograph of HA nanoparticle. The inset shows TEM micrograph of the "necklace bead model" scaffolds. E) Typical single point experimental absorbance spectrum with ATR correction using FTIR-ATR analyzed in the 675 cm^{-1}–4000 cm^{-1} region: FTIR-ATR plot of the titanate nanowire matrix (bottom) and the "necklace bead model" scaffolds (top). F) Curves of pH versus time for hydroxyapatite-modified titanate nanowire scaffolds by electrochemical method at $I_{appl} = -15$ mA vs SCE and $T = 65$ °C under galvanostatic control.

3.5. Osteoblast adhesion, spreading, proliferation and toxicity

Surface roughness historically was an important element in the design and manufacture of implantable biomedical devices. Particularly in the case of bone implants, roughness was introduced to influence bone ingrowth and early stabilization [44,45]. Titanate nanowire matrix is capable of controlling the surface chemistry as well as macroporous and mechanical

properties. Besides, interconnected macropores of 2–10 μm in diameter could provide a suitable microenvironment for cell differentiation and tissue ingrowth. However, the bioactivity and biocompatibility of the titanate nanowire matrix still need to be improved. The biologically equivalent hydroxyapatite nanostructure on the surface of biomaterials is important for bone healing, which can promote good osteoblast differentiation and subsequent bone formation. In the present study, we investigated the potential of HA nanoparticles to improve the osteogenic action of titanate nanowire matrix, and enhance the *in vitro* formation of bone-like tissues without the osteogenic growth factors.

The "necklace bead model" scaffolds combine the porous nature of titanate nanowire matrix and multifunction of the HA nanostructures, which can promote the formation of biological apatite scaffold and accelerate the growth of tissue around the implant materials [46]. Moreover, the micro-texturing of macroporous biomaterials could load cell and induce bone formation in non-osseous environment [15,47]. For the target tissue, in order to

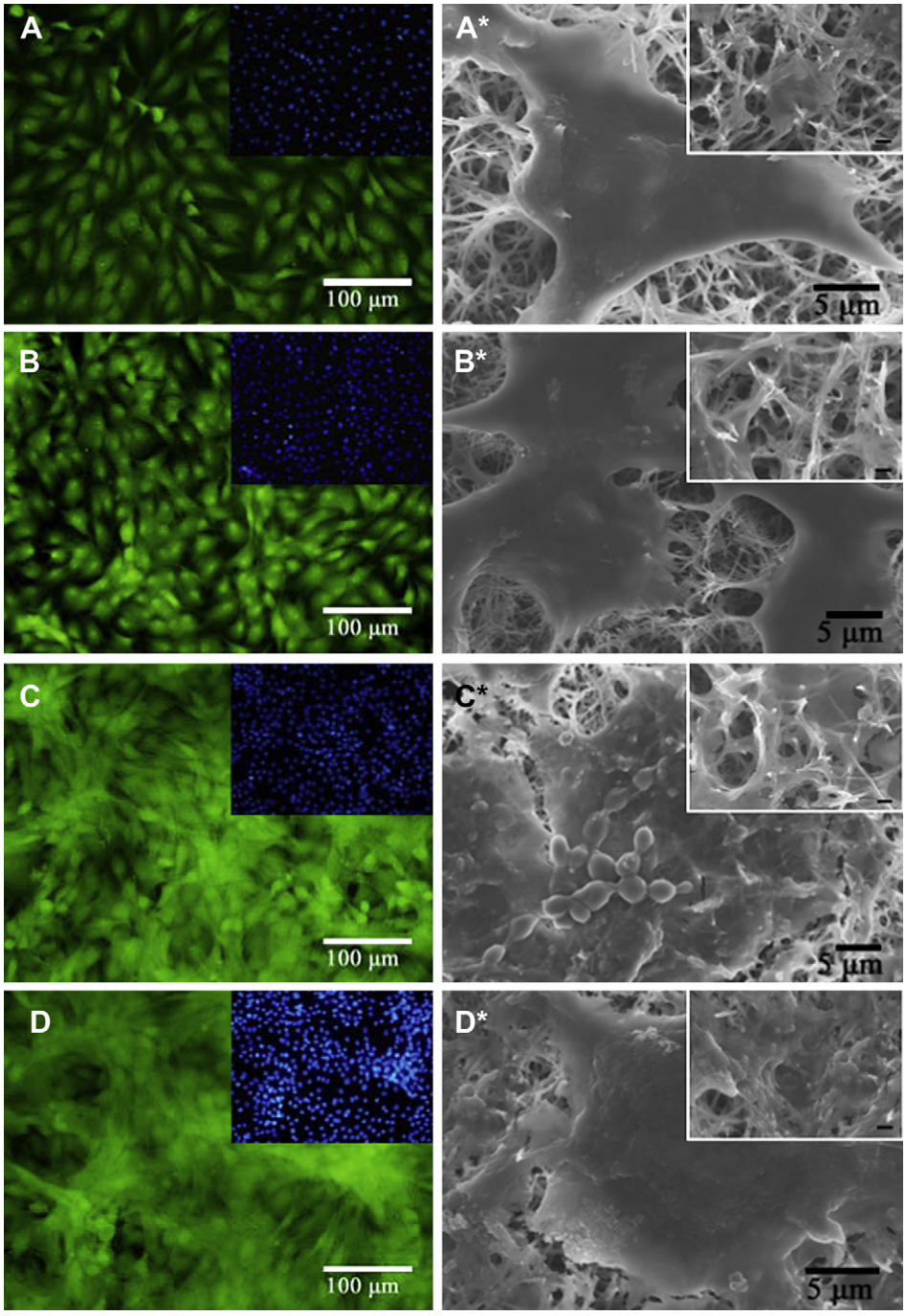

Fig. 5. Fluorescence microscopy and FESEM images of attachment of MG63 cells (green, labeled with phalloidin-FITC, counterstained with DAPI for unclei in blue) on the "necklace bead model" scaffolds: A–D) Fluorescence microscopy survey images of attachment of MG63 cells with different cell seeding time of 1, 3, 5 and 7 days, respectively. The insets show the unclei of MG63 cells. A*–D*) FESEM survey images of attachment of MG63 cells on the "necklace bead model" scaffolds with four different cell seeding time 1, 3, 5 and 7 days, respectively. The insets show the attachment of MG63 cells on the macroporous of the "necklace bead model" scaffolds (scalbar 200 nm). (For interpretation of the references to colour in this figure legend, the reader is referred to the web version of this article.)

check the effect of "necklace bead model" scaffolds and titanate nanowire matrix, MG63 human osteoblast cells were used to evaluate the cellular compatibility, proliferation, and ALP activity. The same standard of samples was chosen for the *in vitro* testing on the desired morphology and properties (the optimization condition: pH = 8.60, $I_{appl} = -15$ mA, $T = 65$ °C and $t = 3$ h). Figs. 5 and 6 show the MG63 cell attachment and proliferation on the "necklace bead model" scaffolds and titanate nanowire matrix. Osteoblast growth in material-free organ culture can be distinguished into four stages, namely cells adhesion, attachment, spreading and proliferation. After cell attachment, the osteoblasts began a period of rapid proliferation, which was confirmed by the difference of the cell number between 3 and 7 days on the "necklace bead model" scaffolds and titanate nanowire matrix. The fluorescence microscopy images of live cells on the "necklace bead model" scaffolds incubated with MG63 cells for 1, 3, 5 and 7 days are shown in Fig. 5A–D, respectively. The live cells on the "necklace bead model" scaffolds appear as viridity spots and related cytoblast as purplish blue spots. These features confirm that the biocompatible "necklace bead model" scaffolds exhibit superior adhesion and bioactivity to MG63 cells than titanate nanowire matrix. It is believed that the HA nanostructure coating may provide dense population of cellular binding sites and the scaffold can offer ample space for tissue cell ingrowth, which are the major criteria to realize enhanced cellular activity and biocompatibility of the materials [48–50]. Fig. 5A*–D* show the FESEM images of MG63 cells cultured on the "necklace bead model" scaffolds accordingly. The MG63 cells became confluence on top of the "necklace bead model" scaffolds after 7 days of culture. For 1 day of culture, the attachment points for MG63 cells did not show sharp difference between two types of the scaffolds. However, after 3 days culture, the titanate nanowires and HA nanoparticles of the "necklace bead model" scaffolds were laid down by MG63 cells. Further, larger areas of cell attachment were observed on the "necklace bead model" scaffolds than titanate nanowire matrix (Supplementary Material Figs. S7 and S8). After 7 days of culture, MG63 cells were attached well and the proliferation yielded cell clusters on the "necklace bead model" scaffolds. FESEM results were in good agreement with the fluorescence microscopy images. The incorporation of nanowire and HA nanostructure with optimal morphology and distribution can increase the biocompatibility and surface roughness of the scaffolds greatly. Moreover, the structure integrity of the "necklace bead model" scaffolds has remained intact after the *in vitro* test.

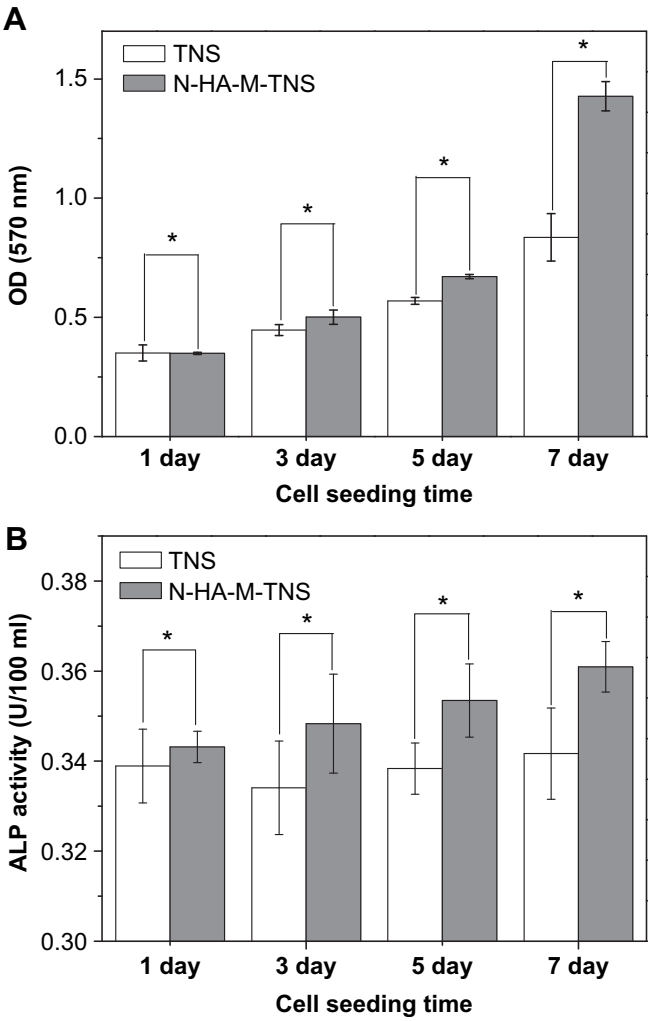

Fig. 6. A comparison of the proliferation and the ALP activity of MG63 cells on the titanate nanowire matrix (TNS) and "necklace bead model" hydroxyapatite-modified titanate nanowire scaffolds (N-HA-M-TNS) after 1, 3, 5 and 7 days of culture (* indicates significance with $p < 0.05$), respectively (the error bar represents the standard deviation).

The biocompatibility and cell viability of the MG63 cells on titanate nanowire matrix and "necklace bead model" scaffolds were further assessed by biochemical approach, and the cellular viability was defined by MTT metabolic assay (Fig. 6A). The MG63 cells presence of better adhesion and proliferation abilities on the "necklace bead model" scaffolds than titanate nanowire matrix due to the modification of the oriented HA nanoparticles. Also, the "necklace bead model" scaffolds could induce the earlier osteoblast differentiation. For 1 day of culture, the cell numbers have not shown significant difference between two types of scaffolds. After 3 days of culture, the number of cells on the "necklace bead model" scaffolds was higher than that on the titanate nanowire matrix, but with not much difference. 7 days of cell culture later, significantly higher cell number was observed on the "necklace bead model" scaffolds than titanate nanowire matrix. The MTT results show that the osteoblast number was lower on titanate nanowire matrix and higher on the "necklace bead model" scaffolds ($p < 0.05$). The oriented HA nanoparticle modification resulted in the rough surface that preferred osteoblast proliferation onto the "necklace bead model" scaffolds. Afterward, the early osteogenic differentiation, bone formation and matrix mineralization were evaluated by ALP activity analyses. In this work, as the cells form multilayered clusters, the rate of their proliferation was decreased and their expression of ALP was increased, followed by the mineralization of natural extracellular matrix. All of the ALP contents of cells on the "necklace bead model" scaffolds were significantly higher than those on titanate nanowire matrix ($p < 0.05$) for 1, 3, 5 and 7 days of culture (Fig. 6B), which indicates that the hydroxyapatite nanoparticles on "necklace bead model" scaffolds can enhance the osteoblastic differentiation of the cells. In particular, there was a larger rise of the ALP activity on "necklace bead model" scaffolds than on titanate nanowire matrix after 7 days of culture. Most notably, cells grown on "necklace bead model" scaffold surface showed significantly higher ALP activity than those on titanate nanowire matrix, which was attributed to not only the enhanced biocompatibility and bioactivity of titanate nanowire matrix, but also the evident surface roughness and large surface area of the scaffolds [51]. Further, all these results confirm that the co-existence of the titanate nanowire core with HA nanoparticle sheath structures are biocompatible and the tissue environment has no undesirable effect.

4. Conclusions

Three dimensional biomimetic "necklace bead model" scaffolds similar to the morphology of the trabecular bone for tissue engineering have been developed by a titanate nanowire matrix assisted electrochemical deposition method. The complex structures and chemical compositions of the scaffolds mimic the natural extracellular matrix. The incorporation of oriented HA nanoparticles with titanate nanowire matrix generates highly osteogenic action, structural integrity, excellently mechanical performance and outstanding cellular compatibility. These interconnected pores could provide a suitable microenvironment for cell growth, tissue cell differentiation and ingrowth. The oriented HA nanoparticle sheath on titanate nanowires, similar to the hierarchical organization of collagen and hydroxyapatite, facilitates the cell attachment and proliferation, and induces the *in vitro* tissue-engineered bone. Human osteoblast-like MG63 cells were cultured on the scaffolds, and the results showed that the scaffolds highly promote the bioactivity, osteoconductivity and osteoblast differentiation.

Acknowledgments

This work was supported by the National Natural Science Foundation of China (Nos. 50972130, 20701033, 50772100, 10874153); Qianjiang Talent Program of Zhejiang Province (QJD1002001); China Postdoctoral Science Foundation (No. 201003048, 20090450292). Open Project Program of State Key Laboratory of Inorganic Synthesis and Preparative Chemistry, Jilin University.

Appendix. Supplementary data

Supplementary data associated with this article can be found, in the online version, at doi:10.1016/j.biomaterials.2011.04.083.

References

[1] Liao S, Cui F, Zhang W, Feng Q. Hierarchically biomimetic bone scaffold materials: nano-HA/Collagen/PLA composite. J Biomed Mater Res Part B 2004; 69:158–65.
[2] Chai C, Leong KW. Biomaterials approach to expand and direct differentiation of stem cells. Mol Ther 2007;15:467–80.
[3] Stevens MM, George JH. Exploring and engineering the cell surface interface. Science 2005;310:1135–8.
[4] Lutolf MP, Gilbert PM, Blau HM. Designing materials to direct stem-cell fate. Nature 2009;462:433–41.
[5] Bakos D, Soldan M, Fuentes IH. Hydroxyapatite-collagen-hyaluronic acid composite. Biomaterials 1999;20:191–5.
[6] Murphy WL, Kohn DH, Mooney DJ. Growth of continuous bonelike mineral within porous poly (lactide-co-glycolide) scaffolds in vitro. J Biomed Mater Res Part A 2000;50:50–8.
[7] Padmanabhan SK, Balakrishana V, Lee YJ, Chu MC, Kim TN, Cho SJ. Sol–gel synthesis and characterization of hydroxyapatite nanorods. Particuology 2009;7:466–70.
[8] Manso M, Jiménez C, Morant C, Herrero P, Martínez-Duart JM. Electrodeposition of hydroxyapatite coatings in basic conditions. Biomaterials 2000;21: 1755–61.
[9] Lu Y, Li M, Li S, Wang Z, Zhu R. Plasma-sprayed hydroxyapatite+titania composite bond coat for hydroxyapatite coatingon titanium substrate. Biomaterials 2004;25:4393–404.
[10] Wei M, Ruys AJ, Swain MV, Kim SH, Milthorpe BK, Sorrell CC. Interfacial bond strength of electrophoretically deposited hydroxyapatite coatings on metals. J Mater Sci Mater Med 1999;10:401–9.
[11] Gomez-Vega JM, Saiz E, Tomsia AP, Oku T, Suganuma K, Marshall GW, et al. Novel bioactive functionally graded coatings on TI6Al4V. Adv Mater 2000;12: 894–8.
[12] Zhang H, Yan Y, Wang Y, Li S. Thermal stability of hydroxyapatite whiskers prepared by homogenous precipitation. Adv Eng Mater 2002;4:916–9.
[13] Dong W, Zhang T, Epstein J, Cooney L, Wang H, Li Y, et al. Multifunctional nanowire bioscaffolds on titanium. Chem Mater 2007;19:4454–9.
[14] Daculsi G, LeGeros RZ, Heughebaert M, Barbieux I. Formation of carbonateapatite crystals after implantation of calcium phosphate ceramics. Calcif Tiss Int 1990;46:20–7.
[15] Hu R, Lin CJ, Shi HY. A novel ordered nano hydroxyapatite coating electrochemically deposited on titanium substrate. J Biomed Mater Res Part A 2007; 80:687–92.
[16] Soballe K. Hydroxyapatite ceramic coating for bone implant fixation. Acta Orthop Scand Suppl 1993;255:1–58.
[17] Gao HJ, Ji BH, Jäger IL, Arzt E, Fratzl P. Materials become insensitive to flaws at nanoscale: lessons from nature. PNAS 2003;100:5597–600.
[18] Moreau JE, Anderson K, Mauney JR, Nguyen T, Kaplan DL, Rosenblatt M. Tissue-engineered bone serves as a target for metastasis of human breast cancer in a mouse model. Cancer Res 2007;67:10304–8.
[19] Reichert JC, Quent VM, Burke LJ, Stansfield SH, Clements JA, Hutmacher DW. Mineralized human primary osteoblast matrices as a model system to analyse interactions of prostate cancer cells with the bone microenvironment. Biomaterials 2010;31:7928–36.
[20] Kothapalli CR, Shaw MT, Wei M. Biodegradable HA-PLA 3-D porous scaffolds: effect of nano-sized filler content on scaffold properties. Acta Biomater 2005; 1:653–62.
[21] Zhang S. Fabrication of novel biomaterials through molecular self-assembly. Nat Biotechnol 2003;21:1171–8.
[22] Suh JK, Matthew HW. Application of chitosan-based polysaccharide biomaterials in cartilage tissue engineering: a review. Biomaterials 2000;21:2589–98.
[23] Zhang Y, Zhang M. Three-dimensional macroporous calcium phosphate bioceramics with nested chitosan sponges for load-bearing bone implants. J Biomed Mater Res Part A 2002;61:1–8.
[24] Kawai N, Niwa S, Sato M, Sato Y, Suwa Y, Ichihara I. Bone formation by cells from femurs cultured among three-dimensionally arranged hydroxyapatite granules. J Biomed Mater Res Part A 1997;37:1–8.
[25] Brandt J, Henning S, Michler G, Schulz M, Bernstein A, Schulz M. Nanocrystalline hydroxyapatite for bone repair: an animal study. J Mater Sci Mater Med 2010;21:283–94.
[26] Shors E, Holmes R. In: Hench LL, Wilson J, editors. Porous hydroxyapatite. An introduction to bioceramics. Singapore: World Scientific; 1993. p. 181–98.
[27] Hanzu I, Djenizian T, Ortiz GF, Knauth P. Mechanistic study of Sn electrodeposition on TiO_2 nanotube layers: thermodynamics, kinetics, nucleation, and growth modes. J Phys Chem C 2009;113:20568–75.
[28] Natarajan C, Nogami G. Cathodic electrodeposition of nanocrystalline titanium dioxide thin films. J Electrochem Soc 1996;143:1547–50.
[29] Rabiee S, Moztarzadeh F, Solati-Hashjin M. Synthesis and characterization of hydroxyapatite cement. J Mol Struct 2010;969:172–5.
[30] Palazzo B, Iafisco M, Laforgia M, Roveri N, Natile G, Bianchi CL, et al. Biomimetic hydroxyapatite–drug nanocrystals as potential bone substitutes with antitumor drug delivery properties. Adv Funct Mater 2007;17:2180–8.
[31] Barrere F, Blitterswijk CA, Groot KD, Layrolle P. Nucleation of biomimetic Ca–P coatings on Ti6Al4V from a SBF×5 solution: influence of magnesium. Biomaterials 2002;23:2211–20.
[32] Kumta PN, Sfeir C, Lee DH, Choi D. Nanostructured calcium phosphates for biomedical applications: novel synthesis and characterization. Acta Biomater 2005;1:65–83.
[33] Hou C, Hou S, Hsueh YS, Lin J, Wu H, Lin F. The *in vivo* performance of biomagnetic hydroxyapatite nanoparticles in cancer hyperthermia therapy. Biomaterials 2009;30:3956–60.
[34] Ma G, Liu X. Hydroxyapatite: hexagonal or monoclinic? Cryst Growth Des 2009;9:2291–4.
[35] Rehman I, Bonfield W. Characterization of hydroxyapatite and carbonated apatite by photo acoustic FTIR spectroscopy. J Mater Sci Mater Med 1997;8:1–4.
[36] Leyva AG, Marrero J, Smichowski P, Cicerone D. Sorption of antimony onto hydroxyapatite. Environ Sci Technol 2001;35:3669–75.
[37] Wilson RM, Elliott JC, Dowker SEP, Smith RI. Rietveld structure refinement of precipitated carbonate apatite using neutron diffraction data. Biomaterials 2004;25:2205–13.
[38] Füredi-Milhofer H, Brecevic L, Purgaric B. Crystal growth and phase transformation in the precipitation calcium phosphates. Faraday Discuss Chem Soc 1976;61:184–93.
[39] Han Y, Fu T, Lu J, Xu K. Characterization and stability of hydroxyapatite coatings prepared by an electrodeposition and alkaline-treatment process. J Biomed Mater Res Part A 2001;54:96–101.
[40] Nie X, Leyland A, Matthews A, Jiang J, Meletis EI. Effects of solution pH and electrical parameters on hydroxyapatite coatings deposited by a plasma-assisted electrophoresis technique. J Biomed Mater Res Part A 2001;57:612–8.
[41] Naldoni A, Minguzzi A, Vertova A, Santo VD, Borgese L, Bianchi CL. Electrochemically assisted deposition on TiO_2 scaffold for tissue engineering: an apatite bio-inspired crystallization pathway. J Mater Chem 2011;21:400–7.
[42] Yen SK, Lin C. Cathodic reactions of electrolytic hydroxyapatite coating on pure titanium. Mater Chem Phys 2002;77:70–6.
[43] Yuan Q, Golden TD. Electrochemical study of hydroxyapatite coatings on stainless steel substrates. Thin Solid Films 2009;518:55–60.
[44] Wu Y, Zitelli JP, Libera MR, Tenhuisen KS, Yu XJ. Differential response of staphylococci and osteoblasts to varying titanium surface roughness. Biomaterials 2011;32:951–60.
[45] Yang P, Quan Z, Li C, Kang X, Lian H, Lin J. Bioactive, Luminescent and mesoporous Europium-doped hydroxyapatite as a drug carrier. Biomaterials 2008;29:4341–7.

[46] Bigi A, Boanini E, Bracci B, Facchini A, Panzavolta S, Segatti F, et al. Nanocrystalline hydroxyapatite coatings on titanium: a new fast biomimetic method. Biomaterials 2005;26:4085–9.
[47] Habibovic P, Yuan H, Doel MV, Sees TM, Blitterswijk CAV, Groot KD. Relevance of osteoinductive biomaterials in critical-sized orthotopic defect. J Orthop Res 2006;24:867–76.
[48] Fujii S, Okada M, Sawa H, Furuzono T, Nakamura Y. Hydroxyapatite nanoparticles as particulate emulsifier: fabrication of hydroxyapatite-coated biodegradable microspheres. Langmuir 2009;25:9759–66.
[49] Barrère F, Mahmood TA, Groot KD, Blitterswijk CAV. Advanced biomaterials for skeletal tissue regeneration: instructive and smart functions. Mat Sci Eng R 2008;59:38–71.
[50] Zhang C, Li C, Huang S, Hou Z, Cheng Z, Yang P, et al. Self-activated luminescent and mesoporous strontium hydroxyapatite nanorods for drug delivery. Biomaterials 2010;31:3374–83.
[51] Bhumiratana S, Grayson WL, Castaneda A, Rockwood DN, Kaplan DL, Vunjak-Novakovic G. Nucleation and growth of mineralized bone matrix on silk-hydroxyapatite composite scaffolds. Biomaterials 2011;32:2812–20.